AJNR

Cerebral Necrosis After Radiotherapy and/or Intraarterial Chemotherapy for Brain Tumors: PET and Neuropathologic Studies

Giovanni Di Chiro, Edward Oldfield, Donald C. Wright, Domenic De Michele, David A. Katz, Nicholas J. Patronas, John L. Doppman, Steven M. Larson, Masanori Ito and Conrad V. Kufta

AJNR Am J Neuroradiol 1987, 8 (6) 1083-1091
http://www.ajnr.org/content/8/6/1083

Cerebral Necrosis After Radiotherapy and/or Intraarterial Chemotherapy for Brain Tumors:

PET and Neuropathologic Studies

Giovanni Di Chiro[1]
Edward Oldfield[2]
Donald C. Wright[2]
Domenic De Michele[1]
David A. Katz[3]
Nicholas J. Patronas[1]
John L. Doppman[4]
Steven M. Larson[5]
Masanori Ito[6]
Conrad V. Kufta[2]

Cerebral necrosis after radiotherapy for brain tumors is being recognized as a problem more common than previously estimated. Distinction between this iatrogenic complication and tumor recurrence cannot be made by either CT or MR imaging. By using positron emission tomography (PET) with ^{18}F-deoxyglucose (FDG) we were able to reach a diagnosis of radiation necrosis, later verified, in 10 of 95 patients referred for the purpose of differentiating tumor recurrence from necrosis. The critical PET-FDG feature was focal hypometabolism in the area of necrosis, which contrasted with the hypermetabolism associated with the residual/recurrent tumor.

In addition, four cases of cerebral necrosis after supraophthalmic, intraarterial chemotherapy (BCNU) were studied with the PET-FDG method. The area of chemotherapy damage was also characterized by marked hypometabolism. Histology revealed both similarities and differences between radio- and chemonecrosis.

This article appears in the November/December 1987 issue of *AJNR* and the January 1988 issue of *AJR*.

Received April 14, 1987; accepted after revision June 24, 1987.

Presented in part at the annual meeting of the American Society of Neuroradiology, New Orleans, February 1985.

[1] Neuroimaging Section, National Institute of Neurological and Communicative Disorders and Stroke, Bldg. 10, Rm. 1C-451, National Institutes of Health, Bethesda, MD 20892. Address reprint requests to G. Di Chiro.

[2] Surgical Neurology Branch, National Institute of Neurological and Communicative Disorders and Stroke, National Institutes of Health, Bethesda, MD 20892.

[3] Office of the Clinical Director, National Institute of Neurological and Communicative Disorders and Stroke, National Institutes of Health, Bethesda, MD 20892.

[4] Department of Diagnostic Radiology, The Clinical Center, National Institutes of Health, Bethesda, MD 20892.

[5] Department of Nuclear Medicine, The Clinical Center, National Institutes of Health, Bethesda, MD 20892.

[6] Laboratory of Cerebral Metabolism, National Institute of Mental Health, National Institutes of Health, Bethesda, MD 20892.

***AJNR* 8:1083–1091, November/December 1987**
0195–6108/87/0806–1083

Radiotherapy and, to a lesser degree, chemotherapy are useful, or relatively useful, treatment tools for malignant primary brain tumors [1]. In both therapeutic methods, selective, high-dosage delivery to the tumoral tissue is the obvious strategy for enhancing their efficacy. However, attempts at improving the survival results by "selectivity-enhancing" variations and adjunctions to the conventional radiotherapy and by superselective intracarotid chemotherapy have not been successful [2, 3]. The main limitation is damage to the normal cerebral tissue, a complication still poorly understood despite extensive research efforts reflected in an enormous, almost unmanageable literature. Unresolved remain critical issues such as dosimetry threshold and chronologic development of this iatrogenic lesion, as well as the additive or potentiating effects of radio- and chemotherapy on each other [4, 5].

A fundamental hindrance to a better knowledge of the brain lesions that may follow radio- and/or chemotherapy is the lack of a readily available method to diagnose and follow these complications. For instance, CT [6] and MR imaging [7] have proved essentially useless for differentiating between radiation necrosis and recurrent or residual brain tumor. Even neuropathologic examinations of biopsy material may be inconclusive, with limited sampling being the main diagnostic difficulty. In addition, neuropathology provides only static information and is not suitable for sequential assessment. Only positron emission tomography (PET) with ^{18}F-deoxyglucose (FDG) offers reliable pathophysiologic and diagnostic data in this area [8–11]. Such PET-FDG technology is not, however, available to most practitioners, or even to many investigators involved in the management of patients with brain tumors. In this report we present our results with PET-FDG in cases of cerebral necrosis after radiation and/or intraarterial chemotherapy. It is hoped that the proffered evidence will convince more investigators to adopt and use this valuable research and diagnostic technique. Wider use of PET-FDG is imperative if we wish to reach a more complete understanding of the serious complications related to our therapeutic efforts.

Materials and Methods

The PET studies were carried out with the Neuro-PET [12], a scanner with a full width at half maximum resolution of 6.5 mm (slice thickness, 1.1 cm; pixel size, 2 mm). The patient data are summarized in Tables 1 and 2. The studies include 10 cases of radiation-induced cerebral necrosis (cases 1–10, Table 1), with eight patients treated by conventional radiotherapy and two with a combination of conventional and interstitial radiotherapy. No chemotherapy was used before the PET-FDG study in five of these cases, whereas various types of adjunctive chemotherapy with both IV and intrathecal drug administration were given to the other five patients. In five of the 10 patients, the tumor diagnosis was glioma, while in three cases the neoplasm was metastatic (thyroid carcinoma, Ewing sarcoma, malignant mela-

TABLE 1: Summary of Patients with Postradiation Necrosis

Case No.	Age	Gender	Original Diagnosis/ Original Surgery	Radiation Therapy (Gy)	IV/Intrathecal (IT) Chemotherapy	CT	MR	Time from RT to PET (months)	Survival (months)
1	M	43	Bifrontal glioblastoma multiforme/yes	E: 63	IV: spiromustine, AZQ	+	+	48	After RT: 72[a] After PET: 24
2	M	35	R frontal astrocytoma anaplastic features	E: 57.6	IV: vincristine	+	NP	30	Lost to follow-up
3	M	39	R frontal atypical oligodendroglioma/yes	E: 57.6	Not administered	+	NP	67	After RT: 78 After PET: 11
4	M	70	L temporoparietal glioblastoma multiforme/yes	E: 45 I: 120	Not administered	+	NP	10	After RT: 11 After PET: 1
5	F	40	R frontoparietal astrocytoma anaplastic features/yes	E: 40 I: 200	Not administered	+	NP	14	After RT: 26 After PET: 12
6	F	3	R parietal metastases/yes	E: 61.2	Not administered	+	NP	12	After RT: 60[a] After PET: 48
7	F	20	R frontal and temporoparietal metastases/yes	E: 58	IV: vincristine, adriamycin, cytoxan; IT: methotrexate, ArA C	+	+	12	After RT: 57 After PET: 45
8	M	68	L frontal, R parietal metastases/no	E: 45	IV: CCNU	+	NP	48	After RT: 108
9	M	47	Bifrontal presumptive glioma/no	E: 60	IV:CCNU	+	NP	48	After RT: 84 After PET: 36
10	F	10	Diffuse central nervous system leukemia/no	E: 48	IT: methotrexate IV: ArA C	+	+	72	After RT: 73 After PET: 1

Note.—In all patients, PET findings were cold, and the post-PET pathologic diagnosis was necrosis. RT = radiation therapy; PET = positron emission tomography; R = right; L = left; E = external beam; I = intrathecal; + = positive; NP = not performed.

[a] This patient died.

TABLE 2: Summary of Patients with Postchemotherapy Necrosis

Case No.	Age	Gender	Original Diagnosis/ Original Surgery	Radiation Therapy (Gy)	Intraarterial BCNU (No. of Courses)	Other Chemotherapy	CT	MR	PET Appearance	Time from BCNU to PET (months)	Post-PET Pathologic Diagnosis	Survival (months)
11	44	F	L temporoparietal glioblastoma multiforme/yes	No	220–325 mg (two)	No	+	NP	Cold	2	Necrosis	After BCNU: 5[a] After PET: 3
12	16	M	L temporoparietal glioblastoma multiforme/yes	No	80 mg (two)	IV CCNU	+	+	Mixed	2.5	Necrosis + glioblastoma multiforme	After BCNU: 15[a] After PET: 12.5
13	34	F	R parietal glioblastoma multiforme/yes	50	220 mg (four)	No	+	+	Cold	23	Necrosis	After BCNU: 42 After PET: 19
14	17	F	L temporoparietal glioblastoma multiforme/yes	60	402 mg (four)	No	+	+	Mixed	6	Necrosis, presumed residual glioma	After BCNU: 44 After PET: 38

Note.—PET = positron emission tomography; BCNU = 1,3-bis 2-chloroethyl-1-nitrosourea; L = left; R = right; + = positive; NP = not performed.

[a] This patient died.

noma). In one patient, glioma had been suspected and had been treated without histologic confirmation, and in one case radiation and intrathecal chemotherapy had been instituted for CNS leukemia.

Of some interest is the fact that the 10 cases of postradiation necrosis were recognized in a population of 95 patients referred for a PET-FDG study to differentiate tumor recurrence from necrosis. In the remaining 85 cases, PET-FDG supported the diagnosis of tumor (hypermetabolic focus) and was later verified at surgery and/or autopsy.

Table 2 includes four patients (cases 11–14, all gliomas) studied by PET-FDG after treatment by supraophthalmic, intracarotid infusion of BCNU (1, 3-bis 2-chloroethyl-1-nitrosourea) alone (two cases), or BCNU before (one case) or after (one case) radiotherapy. While no residual or recurrent tumor was encountered in the 10 cases of postradiation necrosis listed in Table 1, two of the four cases of necrosis after intraarterial chemotherapy showed residual tumor (Table 2). In these two patients, the location of the tumor was quite distinct from the areas of necrosis. perhaps reflecting the selectivity of BCNU delivery caused by drug streaming [13, 14]. CT with IV administration of contrast medium was carried out in all of the 14 cases, and MR imaging was performed in six patients. The MR studies did not include administration of Gd-DTPA or other enhancing media. Post-PET neuropathologic verification of necrosis was obtained in all 14 patients, by biopsy in 12 cases and by autopsy in two. In the two cases with residual tumor (Table 2), biopsy verification of the neoplasm was obtained in one.

Finally, in two patients who are not included in Tables 1 and 2, both extensive radiation necrosis and residual and/or recurrent glioma were present. These two patients, in whom tumor as well as necrosis were verified at surgery, are discussed to demonstrate how PET-FDG allows us to recognize discrete tumoral foci within vast areas of necrosis.

All available pathologic material was reviewed by a neuropathologist. The malignant glial tumors were classified according to the scheme described by Burger and Vogel [15], as opposed to the Kernohan system.

Results

In PET-FDG studies, regions of cerebral necrosis are characterized by a reduced glucose utilization rate (Fig. 1). The metabolic values (mg glucose/100 g/min) of the necrotic areas are expressed in FDG activity ratios, comparing uptake in the suspected necrotic areas with activity in an adjacent region and in a corresponding region in the opposite hemisphere when no bilateral extension is evident (Table 3).

The FDG activity ratios of the necrotic areas were consistently low (Table 3), with mean ratios of 0.54 (postradiation) and 0.34 (postchemotherapy), and individual ratios as low as 0.28 (postradiation) and zero (postchemotherapy). In contrast,

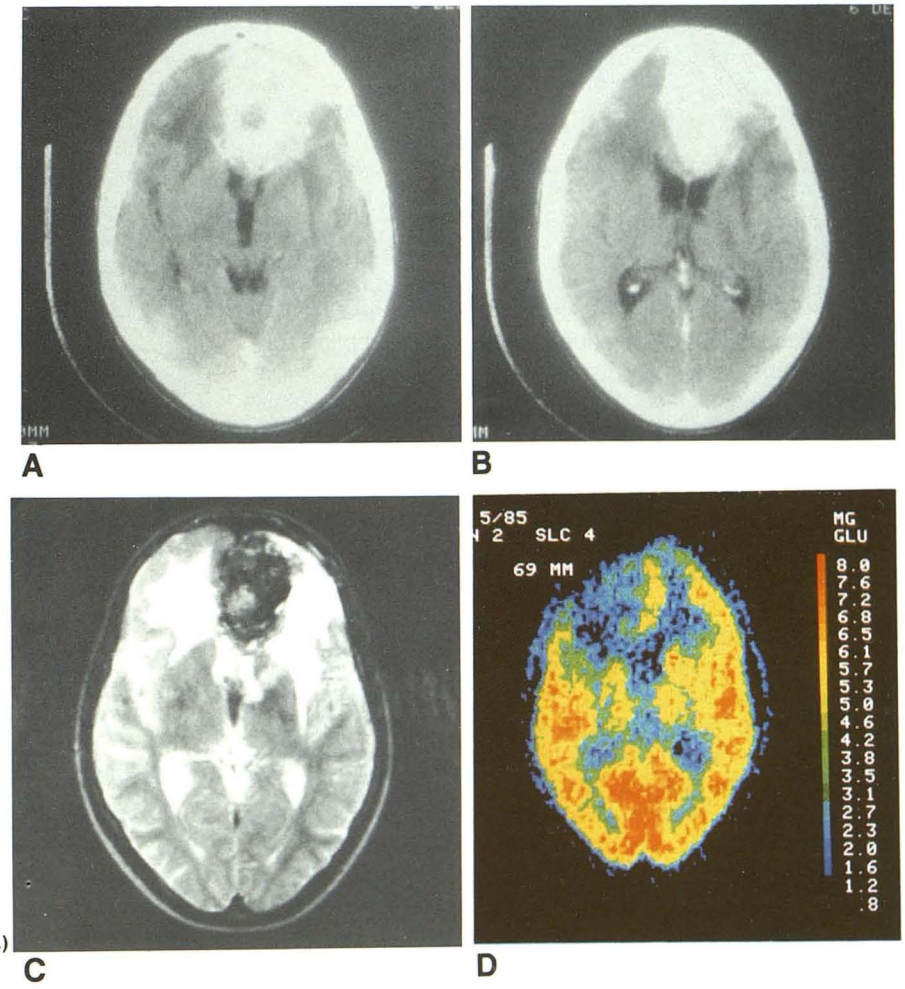

Fig. 1.—Case 1: radiation necrosis.

***A* and *B*, Postcontrast axial CT scans show marked, bifrontal enhancement surrounded by hypodense halo. Lesion is larger on left.**

***C*, MR image (TR = 2500 msec, TE = 120 msec). Mixed-intensity signal from area corresponding to CT enhancement and high-intensity signal from surrounding edema.**

***D*, PET-FDG image at corresponding level. Marked hypometabolism in both prefrontal areas, larger on left. Note selective sparing of interhemispheric gray matter, which is displaced toward right. Color scale indicates range of metabolic values (in mg glucose/100 g/min). (On PET scan only, right side of patient is on right side of image.)**

TABLE 3: ^{18}F-Deoxyglucose Positron Emission Tomographic Metabolic Values in Postradiation and Postchemotherapy Necrotic Lesions

Group: Case No.	Ratio of Lesion to:	
	Adjacent Brain	Corresponding, Contralateral Region
Postradiation necrosis:		
1	0.47	0.78
2	0.70	0.68
3	0.50	0.67
4	0.64	0.62
5	0.28	0.18
6	0.64	0.65
7	0.42	0.40
8	0.66	0.53
9	0.54	0.50
10	0.52	0.49
Mean value	0.54	0.55
Postchemotherapy necrosis:		
11	0.61	0.52
12	0[a]	0
13	0.50	0.34
14	0.26[a]	0.19
Mean value	0.34	0.26

[a] The low values in the necrotic areas contrast with the high ratios (tumor/nontumoral areas) of the residual recurrent neoplasms (ratio of 2.50 for case 12 and 2.84 for case 14).

the ratios of the two residual, recurrent tumors (cases 12 and 14) compared with nontumoral (but not necrotic or obviously edematous) areas were high, 2.50 and 2.84, respectively.

As indicated, in some necrotic areas the metabolic activity was reduced to zero (Fig. 2), reflecting total tissue destruction. In some cases, hypometabolism in necrotic areas could not be differentiated from reduced glucose consumption connected with edematous infiltration, although it appeared that metabolism was somewhat higher in edematous than in necrotic brain. On PET-FDG scans of the postradiation cases, the necrosis was mostly confined to the white matter with sparing of the gray matter (Fig. 1). This pattern, characteristic of radiation necrosis [2, 6, 16], was confirmed at autopsy. Deep gray matter was involved, however, in cases of postintraarterial chemotherapy necrosis. This may have been caused by streaming of the BCNU from the middle cerebral into the lenticulostriate arteries, leading to a selective chemoconcentration and consequent selective damage to the basal ganglia.

In two of our cases with brain injury after selective intraarterial chemotherapy, the limits of the total necrosis are clearly outlined in a background of hemispheric hypometabolism. The area most profoundly affected obviously corresponds to the distribution territory of known perforating arteries (Fig. 2). In other cases, only the diffuse hypometabolic changes involving the entire BCNU-injected hemisphere are demonstrated, without evidence of focality. To explain the diffuse hemispheric hypometabolism, one might invoke, as a causative factor, drug streaming in the distal arterial tree causing widely distributed, discrete areas of tissue damage [14]. These multifocal, scattered areas of injury will appear on the relatively low-resolution PET images as confluent, homogeneous regions of hypometabolism. Another explanation for the widespread hypometabolism of the affected hemisphere may be deafferentation. This phenomenon, which is related to damage of deep structures connected by centrifugal pathways with the cortex [17], may also explain the so-called crossed cerebellar diaschisis (Fig. 3). This is characterized by marked hypometabolism in the cerebellar hemisphere contralateral to the cerebral hemisphere where the primary lesion is located, and may be related either to the original tumor or to the posttherapeutic necrotic lesion [18]. Bilateral, postradiation lesions are often asymmetric (Fig. 4), reflecting the radiation field distribution.

Again and again, in these patients, CT was inadequate to differentiate tumoral from necrotic areas (Figs. 1, 2, and 4). In this respect, we found the MR studies even less informative than CT (Figs. 1 and 2).

Our cases of postradiation necrosis were recognized 10–72 months (mean, 33.1) after the termination of the irradiation. This is in agreement with many previous reports [2, 6, 19, 20]. On the other hand, cerebral necrosis after intraarterial chemotherapy occurred much earlier, at 2–23 months (mean, 8.4 months). This may be because of the concentrated manner of chemotherapeutic administration, which contrasts with the usually fractionated delivery of irradiation over time.

Histopathologically, chemotherapy-induced necrosis resembles the more familiar postradiation tissue damage, with white-matter demyelination, focal coagulation necrosis, reactive gliosis, petechial hemorrhages, and prominent vasculopathic changes. The latter involve particularly small arteries and arterioles and include thickened walls, endothelial proliferation, fibrinoid necrosis, and occlusion alternating with irregular dilatation of the vascular lumen [21]. Notably absent, however, in the postchemotherapy vasculopathy are media and adventitial hyalinization and thin-walled teleangiectasias, two changes rather characteristic of the postradiation pathologic syndrome. In the absence of clinical information, these angiopathic differences are the only features that may assist the neuropathologist in the difficult differential diagnosis between chemotherapy and radiation damage. Finally, the gray matter is affected more often in the chemotherapy lesions than in the radiation damage. This gray matter involvement, however, is partly factitious, related to the selective distribution of the chemotherapeutic compound. In Figures 5 and 6, representative histopathologic patterns of postradiation and postchemotherapy necrosis are illustrated.

Discussion

Suppressed glucose utilization is one of the metabolic alterations that occur after radiation [22, 23]. In a previous study [24], we used the ^{14}C-deoxyglucose autoradiographic method to learn whether radiation administered to rat brain, in a dose below that known to result in any histologic change, may nevertheless affect the brain's local rates of glucose utilization. Measurements were made 4 days and 4 weeks

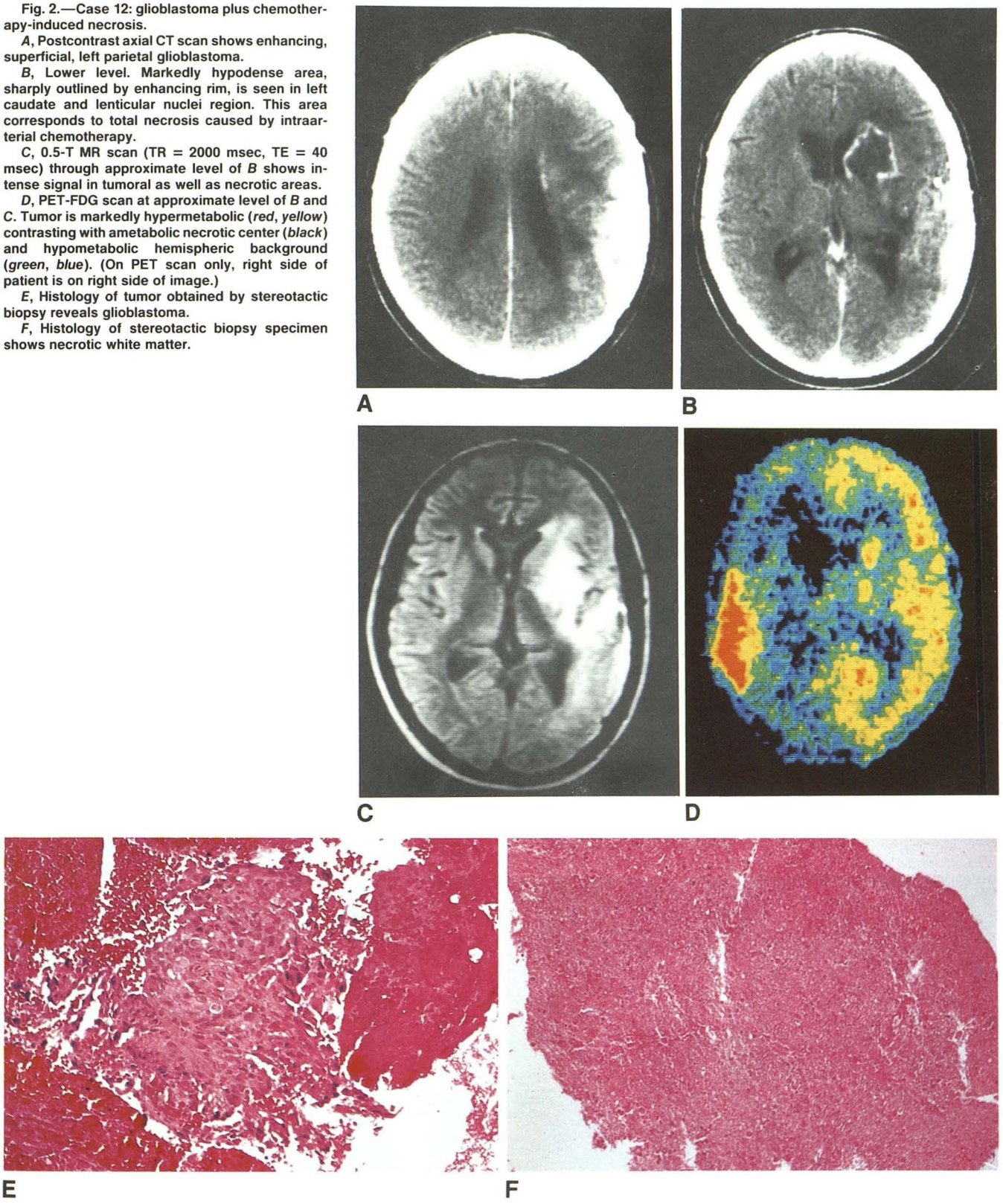

Fig. 2.—Case 12: glioblastoma plus chemotherapy-induced necrosis.

***A*, Postcontrast axial CT scan shows enhancing, superficial, left parietal glioblastoma.**

***B*, Lower level. Markedly hypodense area, sharply outlined by enhancing rim, is seen in left caudate and lenticular nuclei region. This area corresponds to total necrosis caused by intraarterial chemotherapy.**

***C*, 0.5-T MR scan (TR = 2000 msec, TE = 40 msec) through approximate level of *B* shows intense signal in tumoral as well as necrotic areas.**

***D*, PET-FDG scan at approximate level of *B* and *C*. Tumor is markedly hypermetabolic (*red*, *yellow*) contrasting with ametabolic necrotic center (*black*) and hypometabolic hemispheric background (*green*, *blue*). (On PET scan only, right side of patient is on right side of image.)**

***E*, Histology of tumor obtained by stereotactic biopsy reveals glioblastoma.**

***F*, Histology of stereotactic biopsy specimen shows necrotic white matter.**

after exposure of groups of rats to 15 Gy. Rates of glucose utilization in gray- and white-matter structures in both groups were compared with rates in sham-irradiated controls. Statistically significant, lower rates were found in 16 structures 4 days after radiation and in 25 structures 4 weeks after radiation exposure. A weighted average rate for the brain as a whole was 15% below that of the controls for both irradiated groups. In Figure 7, representative ^{14}C-deoxyglucose autoradiographic sections of a control brain and of 4-day and 4-week-postradiation rat brains are illustrated.

Early on in our PET-FDG study of brain tumors we realized that radiation was associated with depressed glucose utilization of the cerebrum as well as of the tumors. We learned to avoid obtaining PET-FDG scans during and soon after radiotherapy in order not to be misled by spuriously low values in the tumoral areas. We also demonstrated that PET-FDG could be used to advantage to differentiate between tumor recurrence from radiation necrosis [8–10]. These findings have been confirmed by other investigators [11]. This report includes our more recent experience with PET-FDG in postradiation necrosis as well as our studies in postintraarterial chemotherapy necrosis. We emphasize that CT and MR scans are essentially useless in the differentiation of tumor vs necrosis. Also, we stress that we have not yet been confronted with a false-positive or a false-negative PET-FDG diagnosis of radiation necrosis. For instance, even when the necrotic changes are overwhelmingly extensive, as in two patients in our series, if a tumoral focus is present, the PET-FDG method will recognize it (Fig. 8). Obviously, diffuse cellular infiltration (paucicellular tumoral spread) may well be beyond the resolving capability of the PET-FDG method.

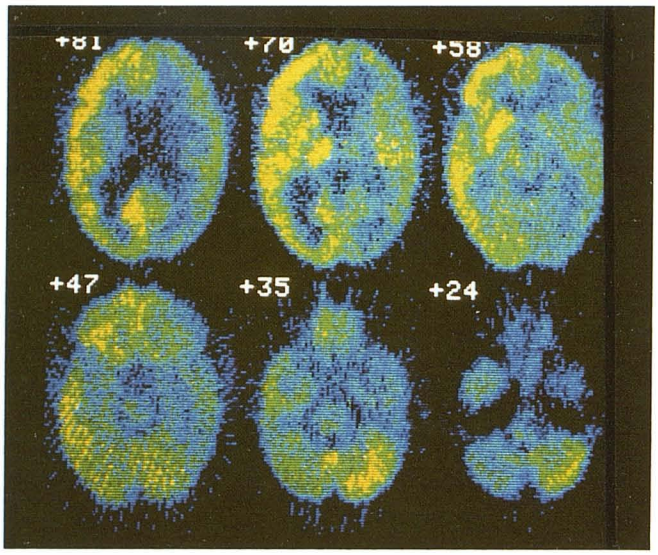

Fig. 3.—Case 13: chemotherapy-induced necrosis. PET-FDG scans show diffuse hypometabolism of entire right cerebral hemisphere (*green*, *blue*). Note that cortex of right cerebellar hemisphere is normometabolic (*yellow*), while left cerebellum is hypometabolic (scans 35 and 24); this phenomenon is referred to as "crossed cerebellar diaschisis." (Right side of patient is on right side of image.)

The dual evidence that radiation affects glucose metabolism and that PET-FDG measures the cerebral glucose metabolic rates and its variations makes this method ideally suited to detect, study, and follow up cerebral radiation damage. In fact, considering the essentially unanimous consensus that neither CT nor MR allows us to reach a diagnosis of radiation necrosis, it is obvious that PET-FDG is one of the few research/diagnostic tools for advancing our knowledge of this iatrogenic complication. Although the amount of information on postchemotherapy necrosis is scanty, we may argue in favor of adopting the PET-FDG technique also for evaluation of this other treatment-related lesion. The similarities between postradiation and postchemotherapy necrosis are probably not surprising [21, 25]. Necrosis, after all, represents a final and common stage for a variety of pathologic processes. The differences in the damage by the two treatment methods perhaps depend on the usually different chronology of the therapeutic regimens, intraarterial therapy being delivered in a shorter time span than radiation is.

In conclusion, PET-FDG is the best diagnostic test currently available for the recognition of cerebral necrosis after radiation and/or chemotherapy and for differentiating necrosis from residual/recurrent tumor. The heuristic importance of the PET-FDG method cannot be overemphasized. The possibility of frequent follow-up studies may allow us to reach a better understanding of the threshold for permanent damage, as well as to sequentially assess the development of necrosis.

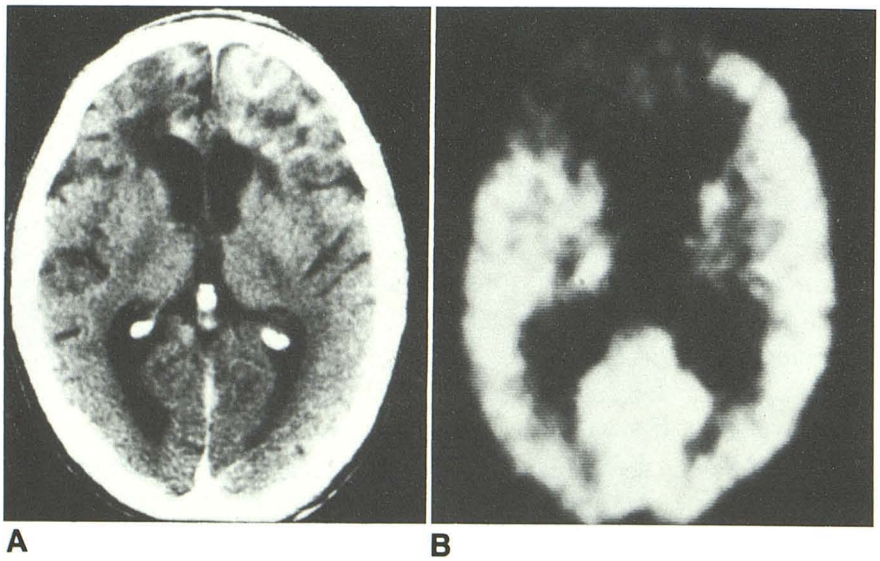

Fig. 4.—Case 8: radiation necrosis.
***A*, Postcontrast axial CT scan shows diffuse changes in both prefrontal areas.**
***B*, PET-FDG scan. Profound hypometabolism in areas corresponding to CT enhancement. Necrotic lesion is larger on left, reflecting radiation field distribution.**

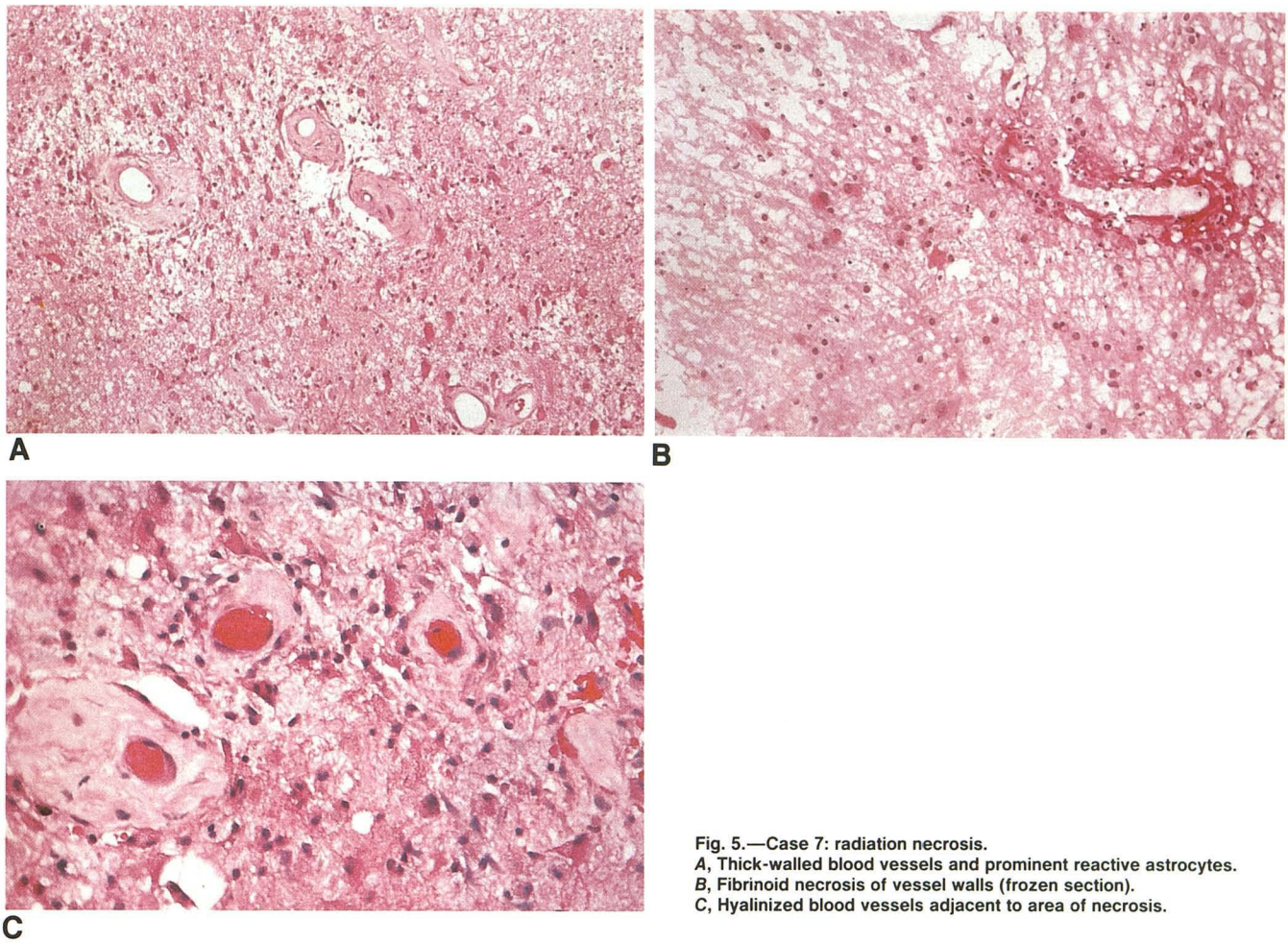

Fig. 5.—Case 7: radiation necrosis.
***A*, Thick-walled blood vessels and prominent reactive astrocytes.**
***B*, Fibrinoid necrosis of vessel walls (frozen section).**
***C*, Hyalinized blood vessels adjacent to area of necrosis.**

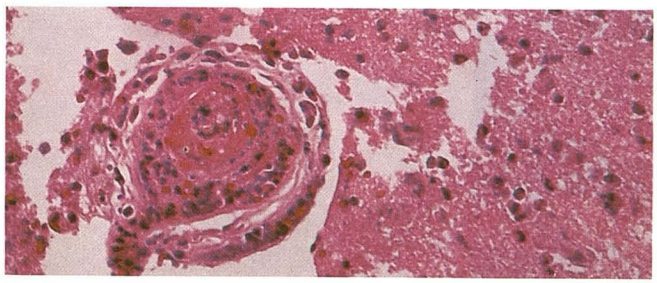

Fig. 6.—Case 14: Chemotherapy necrosis. Note necrotizing vasculitis with transmural inflammation and thrombosis.

REFERENCES

1. Walker MD, Green SB, Byar DP, et al. Randomized comparisons of radiotherapy and nitrosoureas for the treatment of malignant glioma after surgery. *N Engl J Med* **1980**;303:1323–1329
2. Leibel SA, Sheline GE. Radiation therapy for neoplasms of the brain. *J Neurosurg* **1987**;66:1–22
3. Foo SH, Choi IS, Berenstein A, et al. Supraophthalmic intracarotid infusion of BCNU for malignant glioma. *Neurology* **1986**;36:1437–1444
4. Pratt RA, Di Chiro G, Weed JC Jr. Cerebral necrosis following irradiation and chemotherapy for metastatic choriocarcinoma. *Surg Neurol* **1977**;7:117–120
5. Wilson WB, Perez GM, Kleinschmidt-Demasters BK. Sudden onset of blindness in patients treated with oral CCNU and low-dose cranial irradiation. *Cancer* **1987**;59:901–907
6. Martins AN, Johnston JS, Henry JM, Henry JM, Stoffel TJ, Di Chiro G. Delayed necrosis of the brain. *J Neurosurg* **1977**;47:336–345
7. Dooms GC, Hecht S, Brant-Zawadzki M, Berthiaume Y, Norman D, Newton TH. Brain radiation lesions: MR imaging. *Radiology* **1986**;158:149–155
8. Di Chiro G, DeLaPaz RL, Brooks RA, et al. Glucose utilization of cerebral gliomas measured by [^{18}F] fluorodeoxyglucose and positron emission tomography. *Neurology* **1982**;32:1323–1329
9. Patronas NJ, Di Chiro G, Brooks RA, et al. Progress: [^{18}F] fluorodeoxyglucose and positron emission tomography in the evaluation of radiation necrosis of the brain. *Radiology* **1982**;144:885–889
10. Di Chiro G, Patronas NJ, Oldfield EH, Wright DC, Katz DA. PET, CT, and NMR of cerebral necrosis following radiotherapy or intra-arterial chemotherapy for cerebral tumors. *AJNR* **1985**;6:473–474
11. Doyle WK, Budinger TF, Valk PE, Levin VA, Gutlin PH. Differentiation of cerebral radiation necrosis from tumor recurrence by F-18-FDg and Rb-82 positron emission tomography. *J Comput Assist Tomogr* **1987**;11:563–570
12. Di Chiro G, Brooks RA, Bairamian D, et al. Diagnostic and prognostic value of positron emission tomography using [^{18}F] fluorodeoxyglucose in brain tumors. In: Reivich M, Alavi A, eds. *Positron emission tomography*. New York: Liss, **1985**:291–309
13. Lutz RJ, Dedrick RL, Boretos JW, Oldfield EH, Blacklock B, Doppman JL. Mixing studies during intracarotid artery infusions in an in vitro model. *J Neurosurg* **1986**;64:277–283

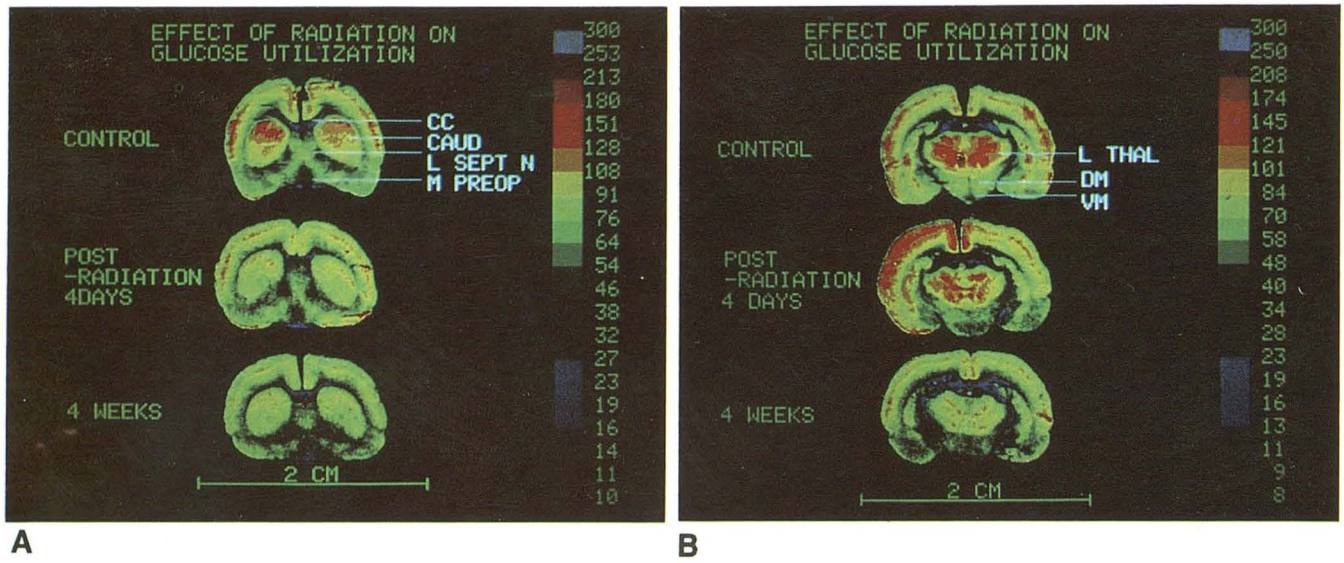

Fig. 7.—^{14}C-deoxyglucose autoradiographs from rat brains (control and 4 days and 4 weeks after irradiation). Bar at right indicates range of rates of glucose utilization (μmol/100 g/min) spanned by each color. Each of the autoradiographs shows three structures displaying rates significantly reduced after irradiation, as compared with those structures in controls. CC = corpus callosum; CAUD = caudate nucleus; L SEPT N = lateral septal nucleus; M PREOP = medial preoptic area; L THAL = lateral thalamic nucleus; DM = dorsomedial nucleus; VM = ventromedial nucleus. Even visually, cerebral metabolic rates in irradiated rats is reduced compared with controls, particularly at 4 weeks after radiation (less red and light yellow, more greenish hue). (Right side of rat is on right side of image.)

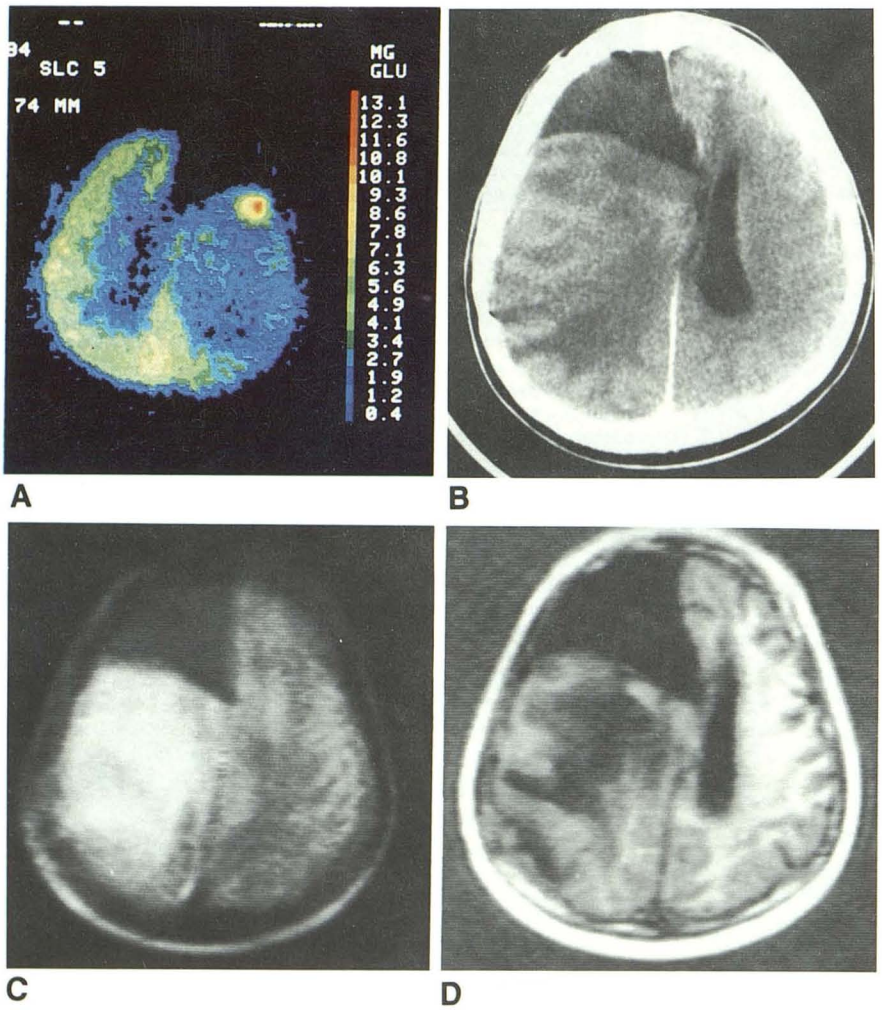

Fig. 8.—Recurrent glioblastoma plus necrosis and edema.

A, PET-FDG scan. Note discrete focus of intense hypermetabolism in right frontal region, behind wedgelike defect caused by previous surgery. Vast areas of hypometabolism (blue) are seen in ipsilateral as well as contralateral hemispheres. These changes are from radiation plus IV chemotherapy injury. Color scale indicates range of metabolic values in mg glucose/100 g/min. (On PET scan only, right side of patient is on right side of image.) Tumor recurrence was not identified on either postcontrast CT scan (*B*) or spin-echo (*C*) or inversion-recovery (*D*) MR images.

14. Blacklock JB, Wright DC, Dedrick RL, et al. Drug streaming during intra-arterial chemotherapy. *J Neurosurg* **1986**;64:284–291
15. Burger PC, Vogel FS. *Surgical pathology of the nervous system and its coverings*, 2d ed. New York: Wiley, **1982**:226–265
16. Davis RL, Robertson DM. *Textbook of neuropathology*. Baltimore: Williams & Wilkins, **1985**:454
17. DeLaPaz RL, Patronas NJ, Brooks RA, et al. Positron emission tomographic study of suppression of gray-matter glucose utilization by brain tumors. *AJNR* **1983**;4:826–829
18. Patronas NJ, Di Chiro G, Smith BH, et al. Depressed cerebellar glucose metabolism in supratentorial tumors. *Brain Res* **1984**;291:93–101
19. Haymaker W, Ibrahim MAM, Miquel J, Call N. Delayed radiation effects in the brains of monkeys exposed to X- and γ-rays. *J Neuropathol Exp Neurol* **1968**;27:50–79
20. Rubinstein LJ. Tumors of the central nervous system. In: *Atlas of tumor pathology*, 2d series, fasc 6. Washington, DC: Armed Forces Institute of Pathology, **1972**:349–360
21. Kleinschmidt-DeMasters BK. Intracarotid BCNU leukoencephalopathy. *Cancer* **1986**;57:1276–1280
22. Hickman J, Ashwell G. Effect of irradiation by X-ray upon anaerobic glycolysis in spleen homogenates. *J Biol Chem* **1953**;205:651–659
23. Parkinson JD, Irving CC. Effect of irradiation on glycolysis of rat liver. *Radiat Res* **1956**;5:589–590
24. Ito M, Patronas NJ, Di Chiro G, Mansi L, Kennedy C. Effect of moderate level X-radiation to brain on cerebral glucose utilization. *J Comput Assist Tomogr* **1986**;10(4):584–588
25. Burger PC, Kamenar E, Schold SC, Fay JW, Phillips GL, Herzig GP. Encephalomyelopathy following high-dose BCNU therapy. *Cancer* **1981**;48:1318–1327